EFFECTS OF MICROPLASTIC CONTENT AND DISTRIBUTION PATTERNS ON SOIL MOISTURE TRANSPORT: AN EXPERIMENTAL AND SIMULATION STUDY

JIANG, G. M.* – ZHANG, H. – XU, J. – HAO, J. H. – LU, J.

College of Civil Engineering and Architecture, Nanyang Normal University, Nanyang 473061, China
(e-mail: 20131112@nynu.edu.cn)

**Corresponding author*
e-mail: jianggengmin2013@126.com

(Received 12th Oct 2025; accepted 14th Jan 2026)

Abstract. In order to explore the effects of microplastic (MP) content and distribution patterns on soil water infiltration and evaporation characteristics, indoor one-dimensional soil column simulation experiments were conducted. Three levels of polyethylene MPs (0.3%, 0.6%, and 0.9%) and two distribution modes (uniform distribution, A; layer-wise decreasing distribution, D) were designed. The applicability of five main infiltration models was evaluated. Results showed that under uniform distribution, soil infiltration and evaporation capacities generally decreased with increasing MPs content, except for the low-content treatment (A3). In contrast, under decreasing layer-by-layer distribution conditions, infiltration and evaporation capacity increased with increasing MPs content. At the same soil depth, the coefficient of variation (CV) of volumetric water content in MPs treatments was generally higher than that in the control (CK). Differences were observed in the time required for volumetric water content to rapidly increase and stabilize among treatments, with A3 requiring the shortest time. Notably, the A3 treatment exhibited the highest cumulative infiltration, increasing by 4.69% compared to CK, and enhanced infiltration and evaporation capacities. The coefficient of determination R^2 for all five models exceeded 0.99, indicating excellent simulation performance. Among them, the Kostiakov and Philip models exhibited higher simulation accuracy, outperforming the Horton model. These findings provide valuable insights for improving water use efficiency and supporting sustainable agricultural ecosystem management.
Keywords: *soil water infiltration, soil moisture evaporation, moisture content, variation coeffcient, model*

Introduction

Microplastics (MPs), as an emerging class of pollutants, have attracted significant research attention worldwide due to their small particle size, resistance to degradation, strong adsorption capacity, and high potential ecological risks (Qi et al., 2020). Soil serves as a major accumulation site for MPs. With the expansion of agricultural practices such as irrigation, plastic mulching, and organic composting, the scope of MPs contamination continues to broaden. One study indicates that long-term plastic-mulched cotton fields can harbor MPs concentrations as high as 1426.67 items·kg^{-1}, posing a severe threat to soil environmental quality and ecosystem health (Liu et al., 2022b). The accumulation of MPs in soil can alter its physicochemical properties and ecological functions, negatively affecting plant growth and potentially entering the food chain, thus posing hazards to human health (Machado et al., 2019; Prata et al., 2020). Artificially applied agricultural mulch film is considered one of the primary sources of MPs in croplands (Yu et al., 2020). In China, mulch films are widely used due to their advantages in retaining soil moisture, providing thermal insulation, and

http://www.aloki.hu ● ISSN 1589 1623 (Print) ● ISSN 1785 0037 (Online)
DOI: http://dx.doi.org/10.15666/aeer/2402_25032521
© 2026, ALÖKI Kft., Budapest, Hungary

increasing crop yield (Bezborodov et al., 2010). Since the introduction of this technology in the arid and semi-arid regions of China during the 1980s, both the area under mulch coverage and the volume of mulch film used have grown substantially (Liu et al., 2022). Nearly 18 million hectares of farmland in China are now cultivated under plastic mulch. However, film recycling remains technically difficult and economically unfeasible. Surveys have shown that residual mulch film in China accounts for approximately 25–33% of the total amount used, predominantly found within the top 0–40 cm of the soil profile. Over time, these residual films degrade into MPs, which then accumulate in the soil (Niu et al., 2016), significantly impacting soil physicochemical properties and microbial community activities (Rillig, 2012).

Soil moisture infiltration refers to the process by which precipitation or irrigation water enters the soil from the surface to become soil moisture. This process plays a vital role in the water cycle of agricultural systems (Schwartz et al., 2019), and largely determines the extent to which soil can effectively utilize irrigation water resources (Wenbo et al., 2009). The accumulation of substantial amounts of MPs in soil can compromise soil structural integrity, thereby influencing soil water dynamics (Liu et al., 2022). For instance, results from laboratory-scale soil column simulation experiments have shown that, as the concentration of MPs increases, the wetting front travels a shorter distance over the same infiltration period, and the advancement rate of the wetting front is significantly reduced (Wang et al., 2022). Liu et al. (2022b) reported that when the concentration of polyethylene (PE) MPs in soil reaches 2%, infiltration performance is notably inhibited. Moreover, the presence of MPs can alter the pathways of soil water transport (Liang et al., 2024), and MPs may migrate under the influence of tillage, leaching, bioturbation, and gravity, resulting in a non-uniform vertical distribution across soil layers (Bo et al., 2023). Gu (2020) differentiated the distribution patterns of residual film and demonstrated that, under the same amount of film residues, a decreasing layer-by-layer distribution exerts a greater inhibitory effect on soil infiltration rate compared to a uniform distribution. Therefore, it is essential to further investigate the influence of varying MPs contents and distribution patterns on soil moisture transport behavior.

Soil evaporation is one of the primary pathways for significant soil moisture loss, which not only leads to the inefficient use of water resources but may also contribute to environmental issues such as the accumulation of pollutants in groundwater (Niu et al., 2016). The accumulation of MPs in soil can induce changes in physical properties, including soil bulk density and water-holding capacity, which may consequently influence the soil moisture evaporation process (Machado et al., 2018). A previous study (Wang et al., 2022) examined the effects of three types of MPs on evaporation in sandy soils and found that MPs inhibited soil water evaporation, with cumulative evaporation decreasing as the concentration of the same type of MPs increased. In contrast, Jannesarahmadi et al. (2023) investigated the effects of two different types of MPs on the evaporation kinetics of sandy soils and reported that MPs enhanced capillary water transport by narrowing soil pore spaces, significantly increasing evapotranspiration and prolonging the constant-rate evaporation phase. These findings suggest that the impact of MPs on soil evaporation processes varies depending on soil type. While most current studies have focused on the effects of MP type, particle size, and concentration, the mechanisms of water transport under the combined influence of MP content and distribution patterns remain insufficiently explored.

http://www.aloki.hu ● ISSN 1589 1623 (Print) ● ISSN 1785 0037 (Online)
DOI: http://dx.doi.org/10.15666/aeer/2402_25032521
© 2026, ALÖKI Kft., Budapest, Hungary

Therefore, this study systematically investigates the mechanisms by which MPs with varying contents and distribution patterns influence water infiltration and evaporation in loamy soil, using indoor one-dimensional soil column simulation experiments. Additionally, the applicability of several widely used infiltration models is evaluated, aiming to provide a scientific foundation for hydrological regulation in MP-contaminated soils and to support the sustainable development of agriculture.

Materials and methods

Materials

The soil used in this experiment was collected in September 2022 from Wolong District, Nanyang City, Henan Province, China, at a depth of 0–50 cm. After removing large impurities such as roots and dead leaves, the soil was air-dried, crushed, and passed through a 2 mm sieve for later use. Soil particle size distribution was determined using a Mastersizer 2000 laser particle size analyzer (Malvern Panalytical Company, UK). According to the analysis, the soil consisted of 7.60% clay, 53.38% silt, and 39.02% sand, and was classified as loam based on the USDA soil texture classification system. The average initial gravimetric water content of the soil was measured as 3.2%. The MPs used in the experiment were in powder form, made of polyethylene (PE)—the same material commonly used in agricultural plastic mulch films. The MPs had a particle size of approximately 150 μm and a spherical shape.

Experimental setup

The apparatus for the soil water infiltration experiment (*Fig. 1*) mainly consisted of soil columns made of polymethyl methacrylate, a Mariotte bottle, and a supporting frame. The soil column had an inner diameter of 20 cm and a height of 70 cm, with an external scale used to observe the position of the wetting front. Openings were made at 10, 20, 30, 40, and 50 cm above the bottom of the column for horizontal insertion of soil moisture and temperature sensors (Logger, L99-TWS-3, China). Small holes were set at the bottom of the soil column to facilitate smooth airflow during infiltration. The Mariotte bottle had an inner diameter of 20 cm and a height of 100 cm, and was equipped with a valve at the bottom. It was connected to the soil column via a plastic hose to provide a constant water head. The volume of infiltrated water was recorded based on the scale marked on the outer surface of the Mariotte bottle.

Experimental design

The experiment was designed with three levels of MPs content, two distribution patterns, and one control treatment (CK), resulting in a total of seven treatments. Each treatment was replicated three times. The MPs contents (MPs weight/soil weight) were set at 0.3%, 0.6%, and 0.9%, and the calculated amounts of MPs added to each treatment were as follows: CK (0 g), A3 (70 g), A6 (141 g), A9 (212 g), D3 (70 g), D6 (141 g), and D9 (212 g), where A denotes Uniform distribution, and D denotes Decreasing layer-by-layer distribution. The proportions of MPs content across soil layers under the two distribution patterns are listed in *Table 1.*

http://www.aloki.hu ● ISSN 1589 1623 (Print) ● ISSN 1785 0037 (Online)
DOI: http://dx.doi.org/10.15666/aeer/2402_25032521
© 2026, ALÖKI Kft., Budapest, Hungary

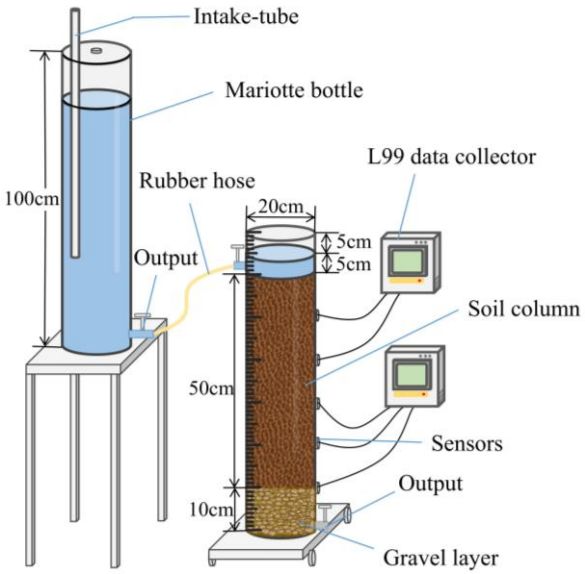

Figure 1. *Schematic diagram of the experimental equipment*

Table 1. *MPs distribution design in different soil layers*

Soil depth (cm)	Proportion of MPs (mass fraction) /% for each soil layer with different distribution	
	Uniform distribution (A)	Decreasing layer-by-layer distribution (D)
0~10	20	34
10~20	20	26
20~30	20	19
30~40	20	13
40~50	20	8

Soil water infiltration

Soil bulk density is 1.50 g/cm^3 and filled in layers. To avoid preferential flow, the inner walls of the columns were coated with Vaseline before filling. The height of the soil in the column was 50 cm, and soil was added in 5 cm increments, with each layer carefully roughened before the next was added to ensure good contact. A 10 cm gravel layer was placed at the bottom as a reverse filter, and covered with filter paper and gauze to prevent the loss of fine particles during infiltration. Vertical infiltration was carried out under a constant head condition, with the water head maintained at 5 cm above the soil surface.

The wetting front movement was recorded using a stopwatch, following the principle of first dense and then sparse timing intervals:0 to 10 min: Once per minute; 10 to 30 min: Once every 4 min; 30 to 60 min: Once every 6 min; 60 to 120 min: Once every 10 min; Thereafter: Once every 15 min until the wetting front reaches a depth of 50 cm. The wetting front depth was determined by averaging measurements from four directions. Meanwhile, soil volumetric water content was automatically recorded every 30 s by sensors, and data were collected for a total of 320 min. After the experiment, the soil columns were sealed.

http://www.aloki.hu ● ISSN 1589 1623 (Print) ● ISSN 1785 0037 (Online)
DOI: http://dx.doi.org/10.15666/aeer/2402_25032521
© 2026, ALÖKI Kft., Budapest, Hungary

Soil moisture evaporation

At the end of the infiltration test the soil columns were left to stand for 24 h for evaporation experiments. The evaporation process was carried out naturally for 30 days in a relatively stable environment in the test site, while evaporation from the water surface was measured using a 20 cm diameter evaporation dish. The mass of the soil columns of each treatment was measured every 24 h by weighing method and the data were averaged three times. The average temperature during the experimental period was 11C° ± 1.9C° and the average humidity was 49.6% ± 6.0% RH. Soil moisture evaporation (W) and evaporation rate (i) were calculated according to the following equations, respectively

$$W = k \times \frac{\Delta M / \rho}{A} \quad \text{(Eq.1)}$$

$$i = \frac{W}{\Delta t} \quad \text{(Eq.2)}$$

where W is the amount of soil moisture evaporated (mm); ΔM denotes the change in mass of the soil column in a given time interval (g); ρ is the density of water (1 g/cm^3); A is the cross-sectional area of the soil column (cm^2); k is the unit conversion factor, k = 10 mm/cm; i is the evaporation rate of soil moisture (mm/d); Δt is the time interval (d).

Model simulation

The relationship between wetting front migration distance and infiltration time is described by a power function (Riquan et al., 2010):

$$F_z = at^b \quad \text{(Eq.3)}$$

where F_z represents the wetting front migration distance (mm); t represents the infiltration time (min); a and b are the dimensionless empirical constants; a represents the wetting front migration distance within the first unit of time; and b represents the attenuation degree of the wetting front process.

The cumulative infiltration was calculated using the following models:

Kostiakov infiltration model (Jha et al., 2019):

$$I = kt^{\beta} \quad \text{(Eq.4)}$$

where I is the cumulative infiltration (mm), and t is the time of infiltration (min), k is the cumulative infiltration of the 1st timing unit (mm), β is the fitted empirical parameter.

Philip infiltration model (Wang et al., 2021):

$$I = St^{0.5} + At \quad \text{(Eq.5)}$$

where S is the soil sorptivity (mm/min), and A is the stable infiltration rate (mm/min).

Horton infiltration mode (Liu et al., 2022):

http://www.aloki.hu ● ISSN 1589 1623 (Print) ● ISSN 1785 0037 (Online)
DOI: http://dx.doi.org/10.15666/aeer/2402_25032521
© 2026, ALÖKI Kft., Budapest, Hungary

$$I = at + \frac{1}{c}(b-a)(1-e^{-ct}) \quad \text{(Eq.6)}$$

where a and b are the presumed final and initial infiltration rates (mm/min), respectively, and c is an empirical constant.

For the water evaporation process, the Rose model was employed for fitting (None, 2010):

$$E = ct_e^{\frac{1}{2}} + dt_e \quad \text{(Eq.7)}$$

where E is the cumulative evaporation (mm), and t_e is the soil moisture evaporation days (d), c is the water diffusion parameter, d is the stable evaporation parameter.

Evaluating indexes of models

The following statistical criteria were used to analyze the efficiency of the model: the relative root mean square error (RRMSE) and the coefficient of efficiency (CE).

$$RRMSE = \frac{\sqrt{\frac{1}{n}\cdot\sum_{i=1}^{n}(S_i - M_e)^2}}{\overline{M_e}} \quad \text{(Eq.8)}$$

$$CE = 1 - \frac{\sum_{i=1}^{n}(S_i - M_e)^2}{\sum_{i=1}^{n}(M_e - \overline{M})^2} \quad \text{(Eq.9)}$$

where n is the number of measured and simulated values, S_i is the model simulation value, M_e is the measured value, and $\overline{M}$ is the mean value of M_e.

The smaller the RRMSE value, the better the model fits, and the closer the CE value is to 1, the more efficient the model simulation is.

Data processing and analysis

The experimental data in this paper are derived from the average values of three replicate experiments. Data processing was performed using Microsoft Office Excel software, while data plotting and function fitting were accomplished using Microsoft PowerPoint and Origin 2024 software. Statistical analysis of the data was conducted using SPSS 25.0 software. Following the identification of significant differences by analysis of variance (ANOVA), Duncan multiple range test was employed for post-hoc comparisons.

Results

Effects of different contents and distribution modes of MPs on the transport of soil wetting peaks

The migration process of the wetting front under different treatments is illustrated in *Figure 2*. During the initial stage of infiltration (first 10 min), the wetting fronts

http://www.aloki.hu ● ISSN 1589 1623 (Print) ● ISSN 1785 0037 (Online)
DOI: http://dx.doi.org/10.15666/aeer/2402_25032521
© 2026, ALÖKI Kft., Budapest, Hungary

advanced rapidly across all treatments, with steep wetting front curves and minimal differences among treatments. As infiltration progressed, the advancement rate of the wetting fronts gradually slowed, the curves became more flattened, and the wetting front migration among treatments remained generally consistent. Among all treatments, A3 exhibited the greatest wetting front depth at a given time and was higher than that of the CK treatment, while A9 showed the shortest wetting front advancement. The times required for the wetting front to reach a depth of 45 cm were as follows: A3 (160 min) < CK (170 min) < D9 (185 min) < A6 (195 min) < D6 (200 min) < D3 (215 min) < A9 (235 min). Notably, the A3 treatment reached the 45 cm depth in the shortest time, which was 5.88% less than that of the CK treatment.

The test results showed that the transport of the wetting front was influenced by both the content and distribution pattern of MPs. Under the condition of Uniform distribution, 0.3% MPs promoted the advancement of the wetting front, whereas when the content exceeded 0.3%, an inhibitory effect was observed, which became more pronounced with increasing content. In contrast, under Decreasing layer-by-layer distribution, all treatments exhibited inhibitory effects on wetting front transport, and notably, the lower the MPs content, the stronger the inhibitory effect.

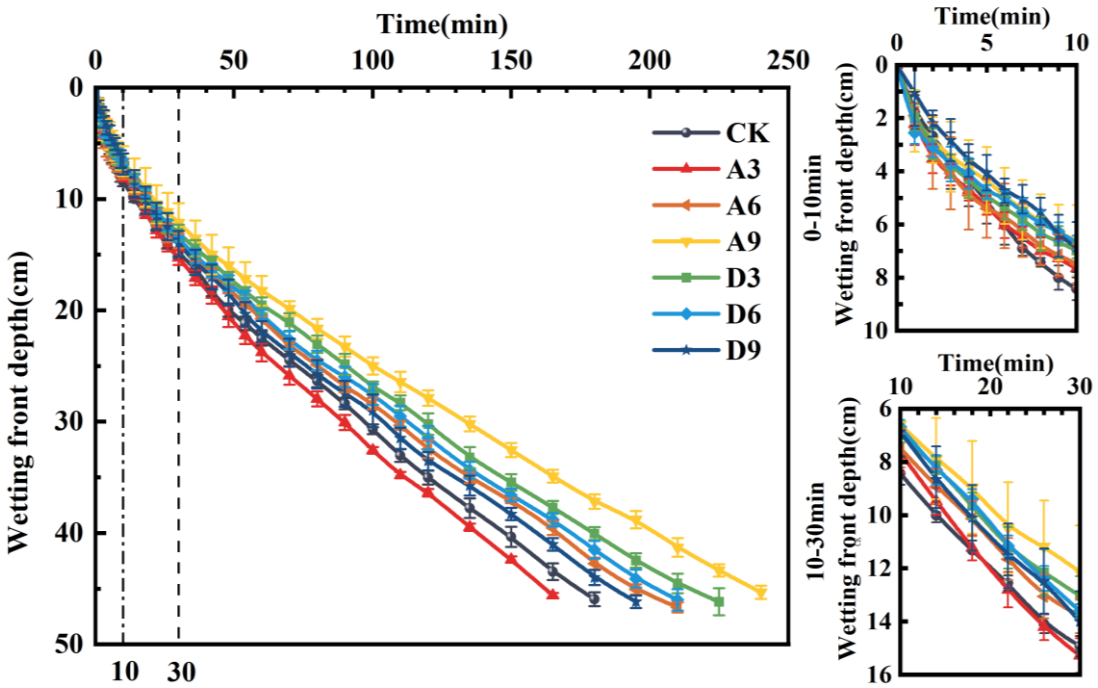

Figure 2. *Dynamic process of wetting front with infiltration time for each treatment*

The fitting parameters of wetting front migration distance and infiltration time are shown in *Table 2*. The coefficients of determination (R^2) for all treatments exceeded 0.99, the coefficient of efficiency (CE) approached 1, and the relative root mean square error (RRMSE) tended toward 0, indicating that the power function model effectively described the transport behavior of the soil wetting front under varying MPs contents and distribution patterns. In the power function, the parameter a represents the initial transport rate of the wetting front, while the parameter b reflects the degree of attenuation in its movement over time (Riquan et al., 2010). Compared to the control

http://www.aloki.hu ● ISSN 1589 1623 (Print) ● ISSN 1785 0037 (Online)
DOI: http://dx.doi.org/10.15666/aeer/2402_25032521
© 2026, ALÖKI Kft., Budapest, Hungary

group without MPs, the treatments with MPs exhibited a notable decrease in the parameter a, indicating that the addition of MPs reduced the initial wetting front transport rate to varying extents. Meanwhile, the parameter b increased significantly, suggesting that the attenuation of wetting front transport was enhanced under the influence of MPs.

Table 2. *The fitting parameters of wetting front migration and infiltration time*

Treatment	*a*	*b*	R^2	RRMSE	CE
CK	1.8631	0.6130	0.9982	0.0290	0.9982
A3	1.8348	0.6225	0.9993	0.0179	0.9993
A6	1.7002	0.6172	0.9983	0.0283	0.9984
A9	1.4310	0.6261	0.9983	0.0292	0.9983
D3	1.5323	0.6268	0.9982	0.0295	0.9983
D6	1.5456	0.6321	0.9989	0.0231	0.9990
D9	1.5250	0.6453	0.9995	0.0166	0.9995

Effects of different contents and distribution patterns of MPs on cumulative soil infiltration and infiltration rates

Figures 3 and *4* show the temporal changes in cumulative infiltration volume and infiltration rate under different MP content and distribution treatments. During the initial infiltration phase (first 10 min), the cumulative infiltration curves for all treatments exhibited steep slopes with minimal inter-treatment variation, consistent with the progression of the wetting front. As infiltration time increased, differences in cumulative infiltration volume gradually emerged among treatments. Overall, treatment A3 maintained higher cumulative infiltration volumes at most observation points, while treatment A9 remained at lower levels. By 120 min, cumulative infiltration volumes differed significantly ($p < 0.05$) among treatments. Among these, treatment A3 exhibited the highest cumulative infiltration volume, showing no significant difference from the CK treatment but significantly higher than all other treatments. Treatment A9 had a cumulative infiltration volume significantly lower than all other treatments. At 120 min, the cumulative infiltration volumes from highest to lowest were: A3 > CK > D9 > A6 > D6 > D3 > A9. Compared to CK, the cumulative infiltration volume in treatment A3 increased by 4.69%, while treatments D9, A6, D6, D3, and A9 decreased by 5.47%, 7.03%, 11.72%, 15.63%, and 22.66%, respectively.

The infiltration rate followed a typical trend of rapid decline during the early phase, followed by a gradual stabilization. This behavior was primarily attributed to the initially low surface soil moisture content, which resulted in high matric suction and consequently a high infiltration rate. As infiltration progressed, increased soil moisture led to a decrease in suction, and the infiltration rate gradually stabilized within approximately 30 min. At 80 min, the infiltration rates under Uniform distribution were ordered as follows: A3 (1.350 mL/min) > CK (1.288 mL/min) > A6 (1.175 mL/min) > A9 (0.975 mL/min). A3 recorded the highest rate, with a 4.81% increase compared to CK, while A6 and A9 decreased by 8.77% and 24.30%, respectively. Under the Decreasing layer-by-layer distribution, the infiltration rates were: CK (1.288 mL/min) > D9 (1.200 mL/min) > D6 (1.100 mL/min) > D3 (1.050 mL/min), all of which were lower than CK by 6.83%, 14.60%, and 18.48%.

http://www.aloki.hu ● ISSN 1589 1623 (Print) ● ISSN 1785 0037 (Online)
DOI: http://dx.doi.org/10.15666/aeer/2402_25032521
© 2026, ALÖKI Kft., Budapest, Hungary

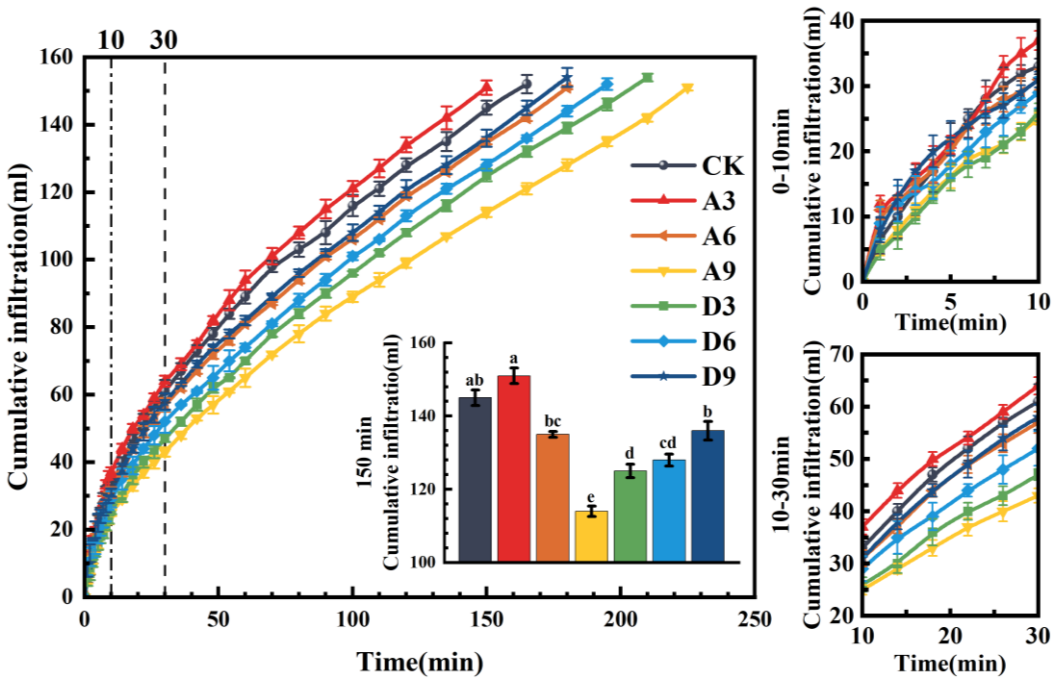

Figure 3. *Dynamics of cumulative infiltration with infiltration time for each treatment. Different lowercase letters indicate significant differences among treatments ($p < 0.05$)*

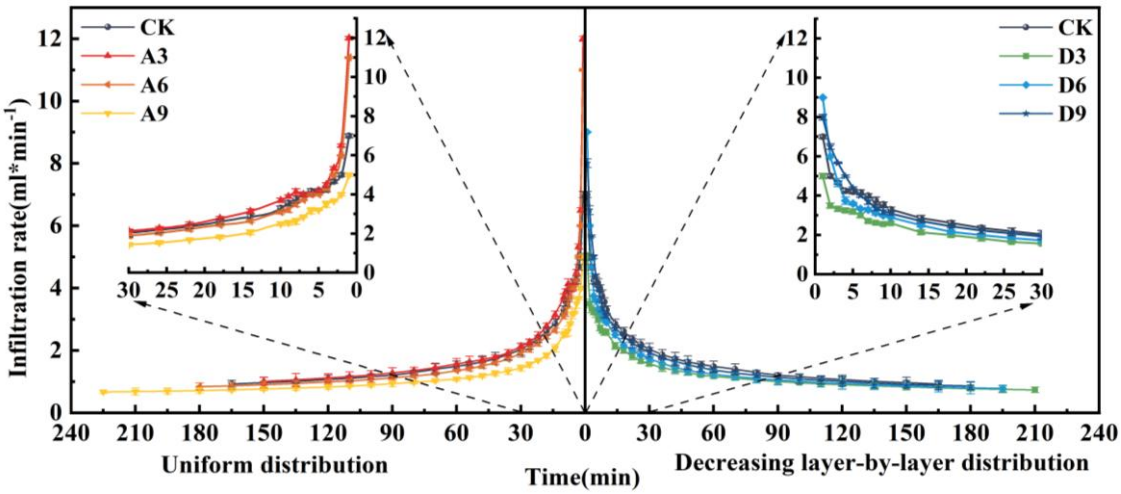

Figure 4. *Dynamic process of soil infiltration rate with infiltration time for each treatment*

Analysis of the cumulative infiltration model

The functional relationship between I and t was expressed by the Kostiakov model, Philip model and Horton model. The fitting parameters and their trends are shown in *Tables 3–5*.

The Kostiakov model fitting results are shown in *Table 3.* under Uniform distribution, the k value generally decreased with increasing MPs content (except for A3), while β increased, indicating a reduction in the initial infiltration capacity and a higher attenuation rate of the cumulative infiltration curve. In contrast, under

http://www.aloki.hu ● ISSN 1589 1623 (Print) ● ISSN 1785 0037 (Online)
DOI: http://dx.doi.org/10.15666/aeer/2402_25032521
© 2026, ALÖKI Kft., Budapest, Hungary

Decreasing layer-by-layer distribution, k increased and β decreased with increasing MPs content, suggesting enhanced initial infiltration and reduced attenuation.

Table 3. *Fitting parameters of Kostiakov model*

Treatment	k	β	R^2	RRMSE	CE
CK	9.4702	0.5441	0.9988	0.0222	0.9988
A3	10.1534	0.5390	0.9986	0.0228	0.9987
A6	8.7644	0.5447	0.9992	0.0177	0.9992
A9	5.6293	0.6021	0.9990	0.0219	0.9990
D3	5.8322	0.6105	0.9995	0.0151	0.9995
D6	7.2549	0.5734	0.9990	0.0204	0.9991
D9	8.9512	0.5438	0.9994	0.0312	0.9977

For the Philip model, *Table 4* indicates that under Uniform distribution, the sorptivity parameter S decreased with increasing MPs content, except for the A3 treatment. In contrast, under Decreasing layer-by-layer distribution, S increased as MPs content increased. The ranking of S values across treatments was A3 > CK > D9 > A6 > D6 > D3 > A9, consistent with the observed trends in wetting front progression and cumulative infiltration. As infiltration progressed, the system entered a steady stage where the stable infiltration rate (A) became dominant (Fu et al., 2009). Under Uniform distribution, A increased with MPs content, whereas under Decreasing layer-by-layer distribution, A declined.

Table 4. *Fitting parameters of Philip model*

Treatment	S	A	R^2	RRMSE	CE
CK	10.3147	0.1246	0.9982	0.0280	0.9981
A3	10.8892	0.1234	0.9983	0.0263	0.9982
A6	9.4703	0.1247	0.9994	0.0164	0.9993
A9	6.8066	0.2079	0.9996	0.0136	0.9996
D3	7.1438	0.2435	0.9992	0.0200	0.9992
D6	8.2450	0.1841	0.9996	0.0141	0.9995
D9	9.6581	0.1247	0.9995	0.0139	0.9995

As illustrated in *Table 5*, under the Horton model, both parameters a and b decreased with increasing MPs content under Uniform distribution but showed an upward trend under Decreasing layer-by-layer distribution. For treatments with low MPs content in Uniform distribution, a and b were higher than those of the CK, suggesting an increased infiltration rate. In treatments A6 and D9, a was lower and b higher than CK, indicating a reduction in early-stage infiltration and an improvement in steady infiltration during the later stages.

Based on R^2, RRMSE, and CE values, the Kostiakov and Philip models demonstrated superior fitting performance compared to the Horton model.

http://www.aloki.hu ● ISSN 1589 1623 (Print) ● ISSN 1785 0037 (Online)
DOI: http://dx.doi.org/10.15666/aeer/2402_25032521
© 2026, ALÖKI Kft., Budapest, Hungary

Table 5. *Fitting parameters of Horton model*

Treatment	*a*	*b*	*c*	R^2	RRMSE	CE
CK	0.6461	4.5451	0.0797	0.9978	0.0301	0.9978
A3	0.7122	5.1329	0.0919	0.9964	0.0376	0.9964
A6	0.6152	4.5827	0.0925	0.9975	0.0321	0.9975
A9	0.5310	3.3007	0.0835	0.9978	0.0326	0.9978
D3	0.5739	3.1356	0.0699	0.9984	0.0282	0.9984
D6	0.6024	4.1258	0.0933	0.9977	0.0318	0.9977
D9	0.6242	4.6447	0.0917	0.9973	0.0485	0.9944

Effects of different MPs contents and distribution patterns on water content of soil profile

As can be seen from *Figure 5A-E*, the soil water content of each treatment in the surface layer (10 cm) of the soil column changed with time in a basically consistent trend, and the profile water curves all changed from a rapid increase to a smooth one, all of them showed a rapid increase in 0–20 min, followed by a gradual stabilization, which indicated that the soil volumetric water content reached saturation rapidly at this stage. In contrast, the water content of each treatment at the depth of the soil column (30 cm) varied significantly with time, with no significant change in the first 80 min. As time passed, the time required for the volumetric water content of each treatment to stabilize from a sudden increase was A3 < CK < D9 < A6 < D6 < D3 < A9, with the A9 treatment lagging significantly behind the other treatments. When the depth of the soil column was greater than 30 cm, the time required for the water content to reach the same depth and stabilize was also in the same order, and the difference gradually increased with time. This trend is consistent with the pattern of wetting front transport and cumulative infiltration, which to a certain extent reflects that both the content and distribution of MPs affect soil water infiltration.

The coefficient of variation (CV) is a parameter that measures the dispersion of related data by comparing the standard deviation to the mean (Chen et al., 2013), and to some extent reflects the variability of soil profile moisture (Cambardella et al., 1994). *Figure 6* shows the CV and average moisture content variation of each soil layer under different content and distribution treatments. Except for the D6 treatment, which exhibited greater variability at the 10–20 cm depth, the CV values for all other experimental groups remained below 15%. This indicates good experimental reproducibility and suggests that the presence of MPs influences the spatial distribution characteristics of soil moisture within the profile to a certain extent.

Effects of different MPs contents and distribution patterns on soil evaporation

The cumulative soil evaporation process under different MP concentrations and distribution patterns is shown in *Figure 6*. During the initial evaporation stage (1–6 days), cumulative evaporation increased rapidly across all treatments, with largely consistent trends and minimal inter-treatment differences. As evaporation progressed, cumulative evaporation differences between treatments gradually emerged. By the end of the evaporation period (30 days), significant differences ($p < 0.05$) were observed

http://www.aloki.hu ● ISSN 1589 1623 (Print) ● ISSN 1785 0037 (Online)
DOI: http://dx.doi.org/10.15666/aeer/2402_25032521
© 2026, ALÖKI Kft., Budapest, Hungary

among treatments. Treatment A3 exhibited the highest cumulative evaporation, though this difference was not significant compared to the CK treatment. Treatments A6, A9, and the stratified decreasing distribution treatment showed overall lower cumulative evaporation than CK, with treatment D3 being significantly the lowest. Compared to CK, the A3 treatment showed a 6.1% increase in cumulative evaporation over 30 days, while treatments A6, A9, D3, D6, and D9 exhibited varying degrees of reduction.

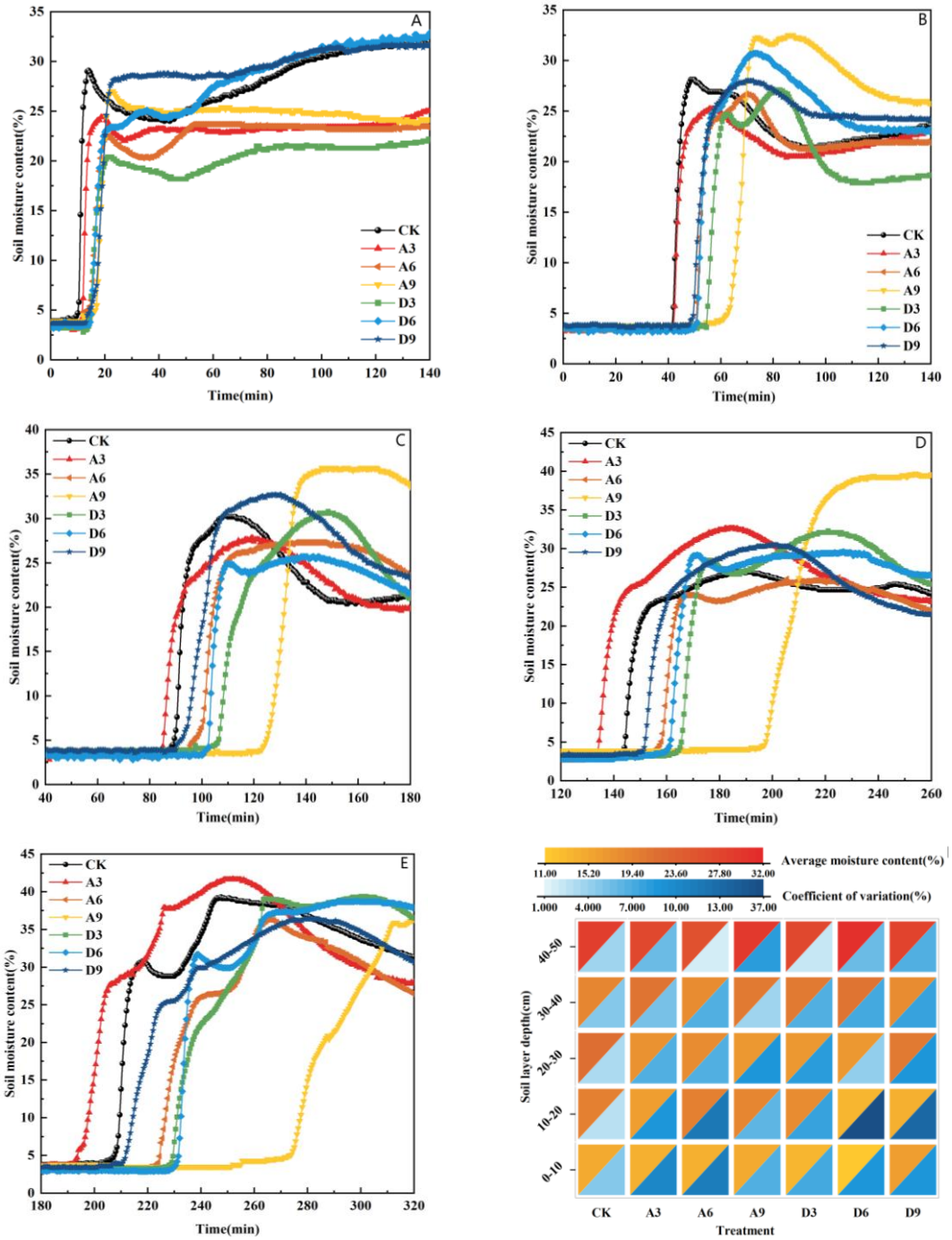

Figure 5. *Changes in volumetric water content of each soil layer over infiltration time, where (A) represents 0–10 cm, (B) represents 10–20 cm, (C) represents 20–30 cm, (D) represents 30–40 cm, (E) represents 40–50 cm, and (F) represents the relationship between average volumetric water content and CV across the soil profile*

http://www.aloki.hu ● ISSN 1589 1623 (Print) ● ISSN 1785 0037 (Online)
DOI: http://dx.doi.org/10.15666/aeer/2402_25032521
© 2026, ALÖKI Kft., Budapest, Hungary

Figure 7 displays the changes in soil evaporation rate under different MPs content and distribution treatments. Evaporation rates were high during the initial stage (days 1–6), primarily driven by environmental factors. The peak evaporation rate under the A3 treatment reached 0.511 mm/d. As soil moisture declined, the evaporation rate gradually decreased in the middle and later stages. Throughout the period, the A3 treatment maintained the highest evaporation rate, with an overall increase of 3.91% compared to CK, while other treatments exhibited reduced rates relative to CK.

The experimental results indicate that, under Uniform distribution, a low MPs content (0.3%) enhanced both cumulative soil evaporation and evaporation rate, whereas higher contents led to reductions, with the degree of reduction increasing alongside MPs content. In contrast, under Decreasing layer-by-layer distribution, lower MPs content produced a stronger inhibitory effect on evaporation. Overall, the cumulative evaporation and evaporation rate followed the descending order: A3 > CK > A6 > D9 > A9 > D6 > D3.

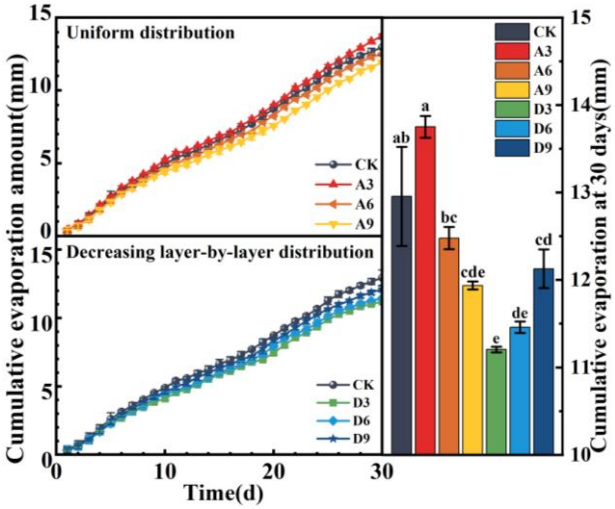

Figure 6. *Cumulative soil evaporation over time under different treatment conditions. Different lowercase letters indicate significant differences among treatments ($p < 0.05$)*

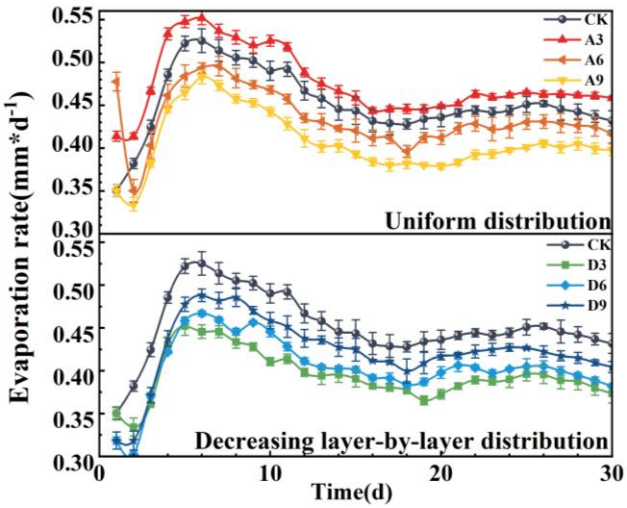

Figure 7. *Changes in soil evaporation rates over time under different treatment conditions*

http://www.aloki.hu ● ISSN 1589 1623 (Print) ● ISSN 1785 0037 (Online)
DOI: http://dx.doi.org/10.15666/aeer/2402_25032521
© 2026, ALÖKI Kft., Budapest, Hungary

The results of the Rose model fitting are presented in *Table 6*. The values of R^2, RRMSE, and CE indicated that the Rose model could accurately simulate the soil evaporation process under different MPs contents and distribution patterns. The parameters *c* and *d* slightly decreased in most treatments compared to CK, except for the A3 treatment, where they showed an increase. These results suggest that under the uniform distribution mode, the water diffusion coefficient first increased and then decreased with rising MPs content. In contrast, under the decreasing layer-by-layer distribution, the water diffusion coefficient increased with MPs content and gradually approached that of CK.

During the stable evaporation stage, the addition of MPs reduced the stable evaporation coefficient in all treatments except A3. This indicates that the inhibitory effect of MPs on soil evaporation primarily occurred during the stable stage, while in the case of low-content MPs under uniform distribution, evaporation was instead promoted during this period.

Table 6. *Fitting parameters of Rose model*

Treatment	*c*	*d*	R^2	RRMSE	CE
CK	0.2122	0.3982	0.9963	0.0318	0.9965
A3	0.2296	0.4127	0.9958	0.0339	0.9959
A6	0.1481	0.3928	0.9960	0.0338	0.9961
A9	0.1452	0.3667	0.9944	0.0396	0.9946
aD3	0.1535	0.3536	0.9964	0.0318	0.9965
D6	0.1857	0.3586	0.9963	0.0323	0.9964
D9	0.1921	0.3779	0.9963	0.0320	0.9965

Discussion

Mechanisms of different MPs contents and distribution patterns on soil infiltration and profile moisture

As an exogenous substance, MPs are fundamentally different from native soil particles due to their hydrophobicity, strong adsorption capacity, and high specific surface area. Once introduced into the soil, MPs can directly alter its physicochemical properties, thereby affecting soil water infiltration (Machado et al., 2018). During infiltration, MPs are subjected to various forces exerted by soil particles, causing them to move along the soil pore network and remain within the soil. Due to their small particle size, large quantities of MPs can accumulate in pore spaces, potentially clogging them and thus impeding water infiltration (Zhou et al., 2021). The impact of MPs on soil infiltration processes is relatively complex. Previous research has also shown that certain chemical substances in the soil solution can bind with pollutants, or that the formation of unstable flow patterns such as “fingers” or “tongues” may accelerate the transport of pollutants within the soil matrix (Xu et al., 2012). These processes can facilitate the movement of more MP particles into soil fractures and pore throats, resulting in the activation of potential preferential flow pathways composed of MPs (Liu et al., 2022), which, in turn, may enhance soil water infiltration. Therefore, the effects of different MPs contents and distribution patterns on soil infiltration are mainly attributed to changes in MP properties, soil pore structure, and infiltration pathways. The ultimate infiltration response depends on the

http://www.aloki.hu ● ISSN 1589 1623 (Print) ● ISSN 1785 0037 (Online)
DOI: http://dx.doi.org/10.15666/aeer/2402_25032521
© 2026, ALÖKI Kft., Budapest, Hungary

dominant relationship among hydrophobic effects, water-blocking effects, and preferential flow formation.

At the early stage of infiltration, the wetting front in each treatment advanced rapidly, with both wetting front and cumulative infiltration curves showing steep trends. This consistency across treatments may result from the dry soil surface quickly reaching saturation, forming a high water potential gradient that accelerated infiltration and minimized treatment differences. As infiltration proceeded, the gradient and infiltration rate declined, and differences among treatments gradually emerged (Wang et al., 2017).

Under Uniform distribution treatment, soil cumulative infiltration decreased with increasing MPs content except for the low-content treatment (A3). This was primarily because high-content MPs uniformly dispersed throughout the soil retained numerous particles within pores, significantly reducing pore connectivity and thereby inhibiting water infiltration. Pore blockage became the dominant factor under these conditions. However, in the A3 treatment, the uniform distribution of low-concentration MPs did not significantly alter the cumulative infiltration volume at 150 min or the cumulative evaporation volume at 30 days. This suggests that when MPs are uniformly distributed at low concentrations, their impact on soil pore structure is minimal, and their influence on soil moisture is limited. Simultaneously, the decrease in infiltration rate with increasing MPs content indicates that even when MPs are uniformly distributed at 9% content, it remains insufficient to form preferential flow pathways that accelerate soil water infiltration. Consequently, increasing MPs content at this stage leads to more pore space being blocked, causing this phenomenon.

Under the decreasing layer-by-layer distribution pattern, soil infiltration capacity generally increased with rising microplastic content (D3 < D6 < D9), yet infiltration rates remained lower than the control group across all treatment groups. This pattern indicates that microplastics primarily accumulate in the topsoil layer. In the low-concentration treatment (D3), the limited amount of surface MPs was insufficient to form continuous preferential flow pathways, allowing pore blockage to dominate and resulting in the greatest suppression of infiltration. As MPs content increased (D6, D9), accumulated surface-layer MPs heightened local hydrophobic effects but simultaneously enhanced the likelihood of forming discontinuous voids or microchannels between particles. This activated “preferential flow pathways,” partially offsetting the negative impact of pore blockage. Consequently, infiltration capacity gradually recovered with increasing content, though it still failed to reach CK levels.

Notably, at identical MPs concentrations, the distribution pattern significantly impacts infiltration more than the concentration itself. For example, infiltration in the A9 treatment (Uniform distribution) was significantly lower than in the D9 treatment (Decreasing layer-by-layer distribution). This occurs because Uniform distribution spreads MPs throughout the entire profile, intensifying pore blockage across the board. In contrast, the Decreasing layer-by-layer distribution concentrates MPs near the surface, allowing lower soil layers to retain relatively intact pore structures and provide conditions conducive to water infiltration. Furthermore, different distribution patterns affect the initial pore structure and profile uniformity of the soil, which further contributes to variations in water movement behavior. Moreover, critical concentration thresholds may exist under both distribution patterns; once microplastic concentrations exceed these thresholds, the aforementioned patterns may undergo transformation.

http://www.aloki.hu ● ISSN 1589 1623 (Print) ● ISSN 1785 0037 (Online)
DOI: http://dx.doi.org/10.15666/aeer/2402_25032521
© 2026, ALÖKI Kft., Budapest, Hungary

Mechanisms of the effects of different MPs content and distribution patterns on soil evaporation

During the evaporation experiment, the cumulative evaporation and evaporation rate curves of all treatments showed a typical trend of being initially steep and later flattening. In the early stage, water supply had just ceased, and the surface soil was near saturation with high hydraulic conductivity. Moisture from deeper layers could effectively replenish surface evaporation losses, resulting in evaporation rates close to those of open water. Additionally, evaporation intensity was susceptible to meteorological factors such as soil temperature, saturation deficit, and wind speed, causing noticeable fluctuations.

As evaporation progressed, the surface layer gradually dried and a desiccation zone formed. The soil transitioned from a saturated to an unsaturated state, leading to a rapid increase in matric suction and a sharp drop in surface vapor pressure. At the same time, the humidity gradient between the soil surface and the surrounding atmosphere decreased, weakening the upward movement of water through soil pores and consequently reducing the evaporation rate, which entered a recession stage (Ou et al., 2016). At this stage, MPs began to influence soil evaporation.

Among the treatments, A3 exhibited higher cumulative evaporation and evaporation rate than D3 and CK, possibly because a low content of MPs under uniform distribution facilitated the formation of preferential pathways. In contrast, under higher contents or decreasing layer-by-layer distribution, MPs blocked a greater number of pores in the surface layer, thereby reducing the effective evaporation area and exerting a suppressive effect. The significant difference between A9 and D9 further indicated that the distribution pattern of MPs played a crucial role in shaping the initial pore structure and uniformity of the soil.

However, other studies have reported that in soils with lower sand content, MPs may bind with soil particles to form new interfacial channels. When such particles accumulate, they may even construct preferential pathways that enhance moisture evaporation (Yong et al., 2019). Therefore, the mechanisms by which MPs content and distribution patterns affect soil water evaporation in different soil types warrant further field-based studies to validate the applicability of these laboratory findings.

Research outlook

Based on an indoor one-dimensional soil column test, this study investigated the effects of different contents and distributions of MPs (represented by 150-micron spherical PE) on the infiltration and evaporation of soil water, which to a certain extent reflected the characteristics of soil water transport under the conditions of MPs storage. In fact, at the early stage of pollution, MPs tended to concentrate and accumulate in the surface layer, forming a similar Decreasing layer-by-layer distribution, at which time water infiltration was significantly inhibited; whereas, under the action of other forces such as long-term leaching, bioturbation, and electrostatic repulsion (Xu et al., 2024), part of the MPs gradually migrated downward over time, and the distribution mode was close to Uniform distribution, and accordingly the infiltration capacity was also changed. However, the indoor experimental conditions differ from the field reality and do not accurately simulate the complex factors such as temperature, humidity, soil structure and water redistribution in the field environment. It is noteworthy that the impact of microplastics on soil hydrological processes is jointly regulated by multiple factors,

http://www.aloki.hu ● ISSN 1589 1623 (Print) ● ISSN 1785 0037 (Online)
DOI: http://dx.doi.org/10.15666/aeer/2402_25032521
© 2026, ALÖKI Kft., Budapest, Hungary

including their own properties and soil texture and compaction status. research indicates that microplastic particle size and soil texture are key factors influencing hydraulic properties (Guo et al., 2022); Wang et al. (2022) found that PP and PVC exhibit stronger infiltration inhibition than PE; while Guo et al. (2025) reported that larger-sized PE exerts a more pronounced effect on the hydraulic properties of compacted soil. Therefore, conclusions are applicable only to the specific conditions of this study. To comprehensively evaluate the long-term effects of MPs on water movement in actual farmland, future work should systematically investigate the environmental behavior and mechanisms of different microplastic properties under complex scenarios.

The relevant research will provide theoretical support for the efficient utilization of farmland water resources and the management of MPs-polluted areas, and contribute to the sustainable development of agroecosystems.

Conclusions

Both MPs distribution mode and content significantly influenced soil water infiltration, with significant differences in cumulative infiltration observed among treatments at 120 min. Under uniform distribution, the low MPs content treatment (A3) exhibited the highest infiltration capacity; however, its cumulative infiltration was not significantly different from CK, while higher MPs contents resulted in a gradual reduction in infiltration. Under the decreasing layer-by-layer distribution, infiltration capacity increased with MPs content but remained generally lower than, and statistically comparable to, CK. The results indicate that MPs generally inhibit soil water infiltration, and the distribution pattern exerts a more significant influence on soil infiltration than their concentration.

MPs altered soil moisture distribution within the soil profile during infiltration. Changes in soil moisture content were consistent with wetting front migration and cumulative infiltration behavior. Among treatments, A3 showed relatively stronger infiltration performance, whereas A9 consistently exhibited the weakest infiltration, reflecting the combined effects of MPs content and spatial distribution.

Cumulative soil evaporation and evaporation rate over the 30-day period differed significantly among treatments. Under uniform distribution, A3 showed the highest evaporation capacity, but its cumulative evaporation was not significantly higher than that of CK, while evaporation decreased with increasing MPs content. Under the decreasing layer-by-layer distribution, evaporation increased with MPs content and gradually approached CK, with several treatments showing no significant difference from CK. These findings further indicate that MPs distribution mode plays a more important role than content in regulating soil evaporation.

Wetting front migration distance followed a power function relationship with time across all treatments. Based on R^2, CE, and RRMSE, the Kostiakov and Philip models adequately simulated cumulative infiltration under different MPs contents and distribution patterns, while the Rose model effectively described soil evaporation dynamics.

Acknowledgements. This work was supported by the National Natural Science Foundation of China (52500163), the Science and Technology Innovation Leading Talent Program of Henan Province (No. 254000510014) and Overseas Expertise Center for Discipline Innovation (No. D23015).

Conflict of interests. The authors declare that there is no conflict of interest.

http://www.aloki.hu ● ISSN 1589 1623 (Print) ● ISSN 1785 0037 (Online)
DOI: http://dx.doi.org/10.15666/aeer/2402_25032521
© 2026, ALÖKI Kft., Budapest, Hungary

REFERENCES

[1] Bezborodov, G. A., Shadmanov, D. K., Mirhashimov, R. T., Yuldashev, T., Qureshi, A. S., Noble, A. D., Qadir, M. (2010): Mulching and water quality effects on soil salinity and sodicity dynamics and cotton productivity in Central Asia. – Agriculture Ecosystems & Environment 138: 95-102. DOI: 10.1016/j.agee.2010.04.005.

[2] Bo, L. J., Li, B., Zhang, K., et al. (2023): Distribution, sources, and behavioral characteristics of microplastics in farmland soil. – Environmental Science 44: 2375-2383. DOI: 10.13227/j.hjkx.202206082.

[3] Cambardella, C. A., Moorman, T. B., Novak, J. M., Parkin, T. B., Karlen, D. L., Turco, R. F., Konopka, A. E. (1994): Field-scale variability of soil properties in central Iowa soils. – Soil Science Society of America Journal 58: 1501-1511. DOI: 10.2136/sssaj1994.03615995005800050033x.

[4] Chen, J., Zheng, X., Qin, Z., Liu, P., Sun, M. (2013): Effects of maize straw mulch on spatiotemporal variation of soil profile moisture and temperature during freeze-thaw period. – Transactions of the Chinese Society of Agricultural Engineering 29(20): 102-110.DOI: 10.3969/j.issn.1002-6819.2013.20.015.

[5] Fu, Q. P., Wang, Q. J., Fan, J. (2009): Comparison among permeability methods of disc infiltrometer. – Transactions of the Chinese Society for Agricultural Machinery 40(9): 56-62.DOI: CNKI:SUN:NYJX.0.2009-09-013.

[6] Gu, Z. D. (2020): Study on the effect and mechanism of residual film amount and residual film distribution on soil water infiltration and evaporation. – Master's Thesis, Shihezi University, Shihezi. DOI: 10.27332/d.cnki.gshzu.2020.001004.

[7] Guo, L., Xu, X., Wang, Q., Park, J., Zhou, L., Lei, H., Wang, X. (2025): Effects of microplastics on the hydraulic properties and pore characteristics of compacted soil. – Soil and Tillage Research 254: 106742. DOI: 10.1016/j.still.2025.106742.

[8] Guo, Z., Li, P., Yang, X., Wang, Z., Lu, B., Chen, W., et al. (2022): Soil texture is an important factor determining how microplastics affect soil hydraulic characteristics. – Environment International 165: 107293. DOI: 10.1016/j.envint.2022.107293.

[9] Jannesarahmadi, S., Aminzadeh, M., Raga, R., Shokri, N. (2023): Effects of microplastics on evaporation dynamics in porous media. – Chemosphere 311: 137023. DOI: 10.1016/j.chemosphere.2022.137023.

[10] Jha, M. K., Mahapatra, S., Mohan, C., Pohshna, C. (2019): Infiltration characteristics of lateritic vadose zones: field experiments and modeling. – Soil and Tillage Research 187: 219-234. DOI: 10.1016/j.still.2018.12.007.

[11] Liang, Y. B., Liu, X. K., Zhai, W. J., Guo, Q. Q., Guo, H. M., Lv, S. C., et al. (2024): Agricultural film-derived microplastics elevate the potential risk of pesticides in soil ecosystem: the inhibited leaching by altering soil pore. – Journal of Hazardous Materials 477: 135210. DOI: 10.1016/j.jhazmat.2024.135210.

[12] Liu, B. S., Li, W. F., Pan, X. L., Zhang, D. Y. (2022a): The persistently breaking trade-offs of three-decade plastic film mulching: microplastic pollution, soil degradation and reduced cotton yield. – Journal of Hazardous Materials 439: 129586. DOI: 10.1016/j.jhazmat.2022.129586.

[13] Liu, Z. H., Cai, L., Dong, Q. E., Zhao, X. L., Han, J. Q. (2022b): Effects of microplastics on water infiltration in agricultural soil on the Loess Plateau, China. – Agricultural Water Management 271: 107818. DOI: 10.1016/j.agwat.2022.107818.

[14] Machado, A. A. D., Lau, C. W., Till, J., Kloas, W., Lehmann, A., Becker, R., Rillig, M. C. (2018): Impacts of microplastics on the soil biophysical environment. – Environmental Science & Technology 52: 9656-9665. DOI: 10.1021/acs.est.8b02212.

[15] Machado, A. A. D., Lau, C. W., Kloas, W., Bergmann, J., Bacheher, J. B., Faltin, E., et al. (2019): Microplastics can change soil properties and affect plant performance. – Environmental Science & Technology 53: 6044-6052. DOI: 10.1021/acs.est.9b01339.

http://www.aloki.hu ● ISSN 1589 1623 (Print) ● ISSN 1785 0037 (Online)
DOI: http://dx.doi.org/10.15666/aeer/2402_25032521
© 2026, ALÖKI Kft., Budapest, Hungary

[16] Niu, W., Zou, X., Liu, J., Zhang, M., Lü, W., Gu, J. (2016): Effects of residual plastic film mixed in soil on water infiltration, evaporation and its uncertainty analysis. – Transactions of the Chinese Society of Agricultural Engineering 32(14): 110-119. DOI: 10.11975/j.issn.1002-6819.2016.14.016.
[17] Ou, B. Q., Tang, C. S., Wang, D. Y., Xu, S. K., Sun, B. (2016): Advances on soil moisture evaporation. – Rock and Soil Mechanics 37(3): 625-636 + 654. DOI: 10.16285/j.rsm.2016.03.003.
[18] Prata, J. C., da Costa, J. P., Lopes, I., Duarte, A. C., Rocha-Santos, T. (2020): Environmental exposure to microplastics: an overview on possible human health effects. – Science of the Total Environment 702: 134455. DOI: 10.1016/j.scitotenv.2019.134455.
[19] Rillig, M. C. (2012): Microplastic in terrestrial ecosystems and the soil? – Environmental Science & Technology 46: 6453-6454. DOI: 10.1021/es302011r.
[20] Rose, C. W. (1966): Agricultural Physics. – Pergamon Press, Oxford. DOI: 10.1016/c2013-0-01995-0.
[21] Schwartz, R. C., Schlegel, A. J., Bell, J. M., Baumhardt, R. L., Evett, S. R. (2019): Contrasting tillage effects on stored soil water, infiltration and evapotranspiration fluxes in a dryland rotation at two locations. – Soil & Tillage Research 190: 157-174. DOI: 10.1016/j.still.2019.02.013.
[22] Shi, R. Q., Cao, G. X., Yang, J., Bo, L., Zhang, R. X., Yang, J. S. (2010): Effects of surface soil mixed with sand on water infiltration and evaporation in laboratory. – Transactions of the Chinese Society of Agricultural Engineering 26(5): 109-114. DOI: CNKI:SUN:NYGU.0.2010-S1-023.
[23] Wan, Y., Wu, C., Xue, Q., et al. (2019): Effects of plastic contamination on water evaporation and desiccation cracking in soil. – Science of the Total Environment 654: 576-582. DOI: 10.1016/j.scitotenv.2018.11.123.
[24] Wang, J., Song, J., Lin, H., Peng, L., Wang, Z. (2021): Comparison of infiltration models to describe infiltration characteristics of bioretention. – Journal of Hydro-environment Research 38: 35-43. DOI: 10.1016/j.jher.2021.08.002.
[25] Wang, J. C., Zhang, B. W., Ni, J. X., Yang, W. H., Li, W. P. (2022): Effect of microplastics on soil water infiltration and evaporation. – Environmental Science 43(8): 4394-4401. DOI: 10.13227/j.hjkx.202111292.
[26] Wang, Z., Li, X., Shi, H., Zhang, D., Xu, P. (2017): Effects of residual plastic film on infiltration and evaporation for sandy loam and sandy soil. – Transactions of the Chinese Society of Agricultural Machinery 48(1): 198-205. DOI: 10.6041/j.issn.1000-1298.2017.01.026.
[27] Wenbo, B., Jiqing, S., Maosong, L., Yafeng, W., Yongfeng, W., Buchun, L., et al. (2009): Effect of super absorbent polymer on vertical infiltration characteristics of soil water. – Transactions of the Chinese Society of Agricultural Engineering 25(2): 18-23.DOI: 10.3864/j.issn.0578-1752.2010.24.009.
[28] Xu, L. H., Wang, Y. H., Wei, F., Dai, Z. X., Zhang, M. (2024): Transport behavior of microplastics in soil-water environments and its dependence on soil components. – Environmental Pollution 346: 123542. DOI: 10.1016/j.envpol.2024.123542.
[29] Xu, Z. H., Xu, Z. M., Cao, J. W., Meng, Q. H. (2012): Research progress of preferential flow in soil. – Soils 44: 905-916. DOI: 10.13758/j.cnki.tr.2012.06.012.
[30] Yu, H., Fan, P., Hou, J. H., Dang, Q. L., Cui, D. Y., Xi, B. D., Tan, W. B. (2020): Inhibitory effect of microplastics on soil extracellular enzymatic activities by changing soil properties and direct adsorption: an investigation at the aggregate-fraction level. – Environmental Pollution 267: 115544. DOI: 10.1016/j.envpol.2020.115544.
[31] Zhou, W., Shi, L., Xu, M. X. (2021): Influence of microplastics on soil water retention. – Journal of Soil and Water Conservation 35(6): 258-263. DOI: 10.13870/j.cnki.stbcxb.2021.06.035.

http://www.aloki.hu ● ISSN 1589 1623 (Print) ● ISSN 1785 0037 (Online)
DOI: http://dx.doi.org/10.15666/aeer/2402_25032521
© 2026, ALÖKI Kft., Budapest, Hungary